CrossMark

Intraseasonal variability of the Atlantic Intertropical Convergence Zone during austral summer and winter

Ana Carolina Nóbile Tomaziello[1] · Leila M. V. Carvalho[2,3] · Adilson W. Gandu[1,4]

Abstract The Atlantic Intertropical Convergence Zone (A-ITCZ) exhibits variations on several time-scales and plays a crucial role in precipitation regimes of northern South America and western Africa. Here we investigate the variability of the A-ITCZ on intraseasonal time-scales during austral summer (November–March) and winter (May–September) based on a multivariate index that describes the main atmospheric features of the A-ITCZ and retains its variability on interannual, semiannual, and intraseasonal time-scales. This index is the time coefficient of the first combined empirical orthogonal function mode of anomalies (annual cycle removed) of precipitation, and zonal and meridional wind components at 850 hPa from the climate forecast system reanalysis (1979–2010). We examine associations between the intraseasonal variability of the A-ITCZ and the activity of the Madden–Julian oscillation (MJO). We show that during austral summer intraseasonal variability of the A-ITCZ is associated with a Rossby wave train in the Northern Hemisphere. In austral winter this variability is associated with the propagation of a Rossby wave in the Southern Hemisphere consistent with the Pacific-South American pattern. Moreover, we show that intense A-ITCZ events on intraseasonal time-scales are more frequent during the phase of MJO characterized by convection over western Pacific and suppression over the Indian Ocean. These teleconnection patterns induce anomalies in the trade winds and upper level divergence over the equatorial Atlantic that modulate the intensity of the A-ITCZ.

1 Introduction

The Intertropical Convergence Zone (ITCZ) is one of the most evident features in the tropics and one of the most extensive convective systems on Earth (Ninomiya 2007). Localized in the ascending branch of the Hadley cell (e.g., Xie and Philander 1994), the ITCZ is a component of the general circulation of the atmosphere (e.g., Citeau et al. 1989; Asnani 1993) and characterizes the meteorological equator (Waliser and Somerville 1994). It plays a crucial role in precipitation regimes in the tropics and affects aviation and cross hemispheric sea routes. From a dynamical perspective, the ITCZ is associated with the equatorial trough and is located in the zone of confluence of the trade winds, where strong convergence of mass forms deep convective clouds (Hastenrath and Lamb 1977; Melo et al. 2009; Souza and Cavalcanti 2009). A number of different methods have been used to investigate the variability of the ITCZ. Most studies identified the ITCZ with indices based on a single variable, usually precipitation (e.g., Sultan and Janicot 2000, 2003; Gu and Adler 2009; Carvalho and Oyama 2013) but other variables such as upper level divergence (Enfield 1996) and sea level pressure (Souza and Cavalcanti 2009) have been used as well.

✉ Ana Carolina Nóbile Tomaziello
carolnobile@model.iag.usp.br

1   Departament of Atmospheric Sciences, University of São Paulo, São Paulo, Brazil

2   Department of Geography, University of California, Santa Barbara, CA, USA

3   Earth Research Institute, University of California, Santa Barbara, CA, USA

4   Research Institute for Meteorology and Water Resources, FUNCEME, Fortaleza, Brazil

The Atlantic ITCZ (A-ITCZ) exhibits variability on a broad range of time-scales: diurnal (Janowiak et al. 1994; Yang and Slingo 2001), synoptic (Diedhiou et al. 1999; Wang and Fu 2007), intraseasonal (Grodsky and Carton 2001; De Souza et al. 2005; Mounier et al. 2008), seasonal (Waliser and Gautier 1993; Carvalho and Oyama 2013), interannual (Moura and Shukla 1981; Nobre and Shukla 1996; Chiang et al. 2002; Rodrigues et al. 2011), and decadal-to-multidecadal (e.g., Zhou and Lau 2001). The annual cycle is, however, the most evident and is characterized by a meridional displacement of the convective band due to the seasonal March of the maximum solar radiation (Asnani 1993). The largest northward (southward) displacement of the A-ITCZ is on average ~14°N (~2°S) between August–September (March–April), which coincides with the wet season in the Sahel (Northeast Brazil) (Wagner 1996).

On synoptic scales the A-ITCZ is typically modulated by easterly wave disturbances (e.g., Carlson 1969; Burpee 1972, 1974; Reed et al. 1977; Thompson et al. 1979; Diedhiou et al. 1999). Easterly waves propagating across the tropical Atlantic are more common during the austral winter and exhibit two distinct regimes with periods between 3–5 days (Reed et al. 1977; Mathon et al. 2002) and 6–9 days (Viltard and De Felice 1979; Viltard et al. 1997). These two regimes distinctly modulate convection in the ITCZ and over Africa (Diedhiou et al. 1999).

Regarding the intraseasonal variability of the A-ITCZ Grodsky and Carton (2001) found oscillations in precipitation on scales between 10 and 15 days during the austral winter and related these oscillations to anomalies in the trade winds. They suggested that these quasi-biweekly oscillations in the A-ITCZ are associated with ocean-atmospheric interactions between tropical Africa and the Atlantic Ocean. Mounier et al. (2008) identified similar pattern of variability, which they referred to as the "quasi-biweekly zonal dipole". They argued that one key mechanism to explain the dipole is the eastward propagation of equatorial Kelvin waves that amplify the pressure gradient between the Atlantic and West Africa and intensify the moisture transport toward the African continent, resulting in a dipole with enhanced convection over Africa and suppressed convection over the A-ITCZ.

De Souza et al. (2005) investigated the intraseasonal variability of precipitation over Northeast Brazil and East Amazon during the austral fall (the rainy season in the region) and showed that the A-ITCZ is one of the main mechanisms driving precipitation variability in these regions on time-scales between 10 and 30 days. They also observed that midlatitude wave trains propagating in the Southern Hemisphere are source of intraseasonal variability of rainfall in the same areas. These results agree with Kiladis and Weickmann (1992) who related convection in the ITCZ to extratropical disturbances.

The Madden–Julian oscillation (MJO) (Madden and Julian 1971, 1994) is considered the most relevant mode of intraseasonal variability in the tropics on time-scales typically between 30 and 90 days (Zhang 2005). Composites of the life cycle of the MJO indicate that the oscillation is associated with a coupled Rossby–Kelvin wave (Gill 1980; Hendon and Salby 1994; Maloney and Hartmann 1998; Matthews 2000; Wheeler and Hendon 2004), which has been related to tropical-extratropical teleconnection patterns on intraseasonal time-scales such as the Pacific North American (PNA) pattern in the Northern Hemisphere (NH) (Wallace and Gutzler 1981) and the Pacific-South American (PSA) pattern in the Southern Hemisphere (SH) (Mo and Higgins 1998). De Souza and Ambrizzi (2006) showed that the MJO modulates convective activity near the equator and affects precipitation over the northeast coast of Brazil, which is a region influenced by the A-ITCZ. The MJO, while the most important, it is not the only source of intraseasonal variability in the atmosphere (Jones and Schemm 2000; Lau and Waliser 2012).

Although these previous studies have contributed to understand the variability of the A-ITCZ on synoptic, inter-annual and decadal time-scales few works have objectively examined variations in the A-ITCZ on intraseasonal time-scales, particularly the importance of tropical-extratropical teleconnections and inter-hemispheric interactions. The goal of this study is to investigate the intraseasonal variability of the A-ITCZ and examine dynamical mechanisms in two seasons: the austral summer (November–March) and austral winter (May–September). To objectively investigate the A-ITCZ we propose a multivariate statistical index based on variables that describe the A-ITCZ behavior and capture the joint variability of convective activity and trade winds on a broad range of time-scales (Sects. 2, 3). We then examine mechanisms associated with intraseasonal variations using band-pass filtered atmospheric variables during the austral summer and winter (Sect. 4). Relationships between the Atlantic ITCZ and the MJO phases are also examined (Sect. 5). A summary of results and the main conclusions are presented in Sect. 6.

2 Data

Circulation at low (850 hPa) and upper levels (200 hPa), and precipitation are examined with the Climate Forecast System Reanalysis (CFSR) from the National Centers for Environmental Prediction (NCEP) (Saha et al. 2010) at 1° horizontal resolution and from 1979 to 2010. To characterize convective activity with an independent variable we use global outgoing longwave radiation (OLR) from

the National Atmospheric and Oceanic Administration (NOAA) (Liebmann and Smith 1996) for the same period with horizontal resolution of 2.5°. Although to this date no specific study has examined the performance of CFSR over the ocean, according to Silva et al. (2011) and Quadro et al. (2012) CFSR is among the best reanalyses representing large-scale precipitation over tropical South America, an improvement that has been attributed to the assimilation of satellite data (Saha et al. 2010). Regardless the wet bias in tropical regions, CFSR data show a good representation of the spatial patterns of precipitation when comparing with Global Precipitation Climatology Project (GPCP) and Tropical Rainfall Measuring Mission (TRMM3B42) date sets (not shown). All data sets are 5-day average (pentad) to eliminate the influence of short-scale variations in the A-ITCZ.

3 Multivariate index for the A-ITCZ

As stated in the introduction, one of our main objectives is to characterize the A-ITCZ with multiple variables to capture the joint variability of convective activity and trade winds. With this purpose we propose an index based on the time coefficient of the first mode of combined empirical orthogonal function (CEOF) analysis of pentad anomalies of the following variables: precipitation, and 850 hPa zonal (U850) and meridional (V850) components of the wind. Details about CEOF can be found in Wilks (2006). Pentad anomalies were obtained by removing the (smoothed) mean annual cycle from the detrended variables at each grid point. As we show next, the A-ITCZ is adequately characterized by combining both precipitation and circulation and the set of variables selected in this study represents the covariability of fields that together provide a good indication of the position and intensity of the convergence zone.

The CEOF domain extends over tropical Atlantic between 45°W–0° longitude and 10°S–10°N latitude (Fig. 1) and includes a small fraction of land over Northeast Brazil and West Africa. The first CEOF (CEOF-1) mode explains about 10 % of the total variance of all variables and is independent of the other modes according to North et al. (1982) test (not shown). Figure 1 shows the spatial pattern of the CEOF-1 as linear correlations between the CEOF-1 time coefficient and the respective time series of the anomalies of each variable at each grid point. The number of independent events considered
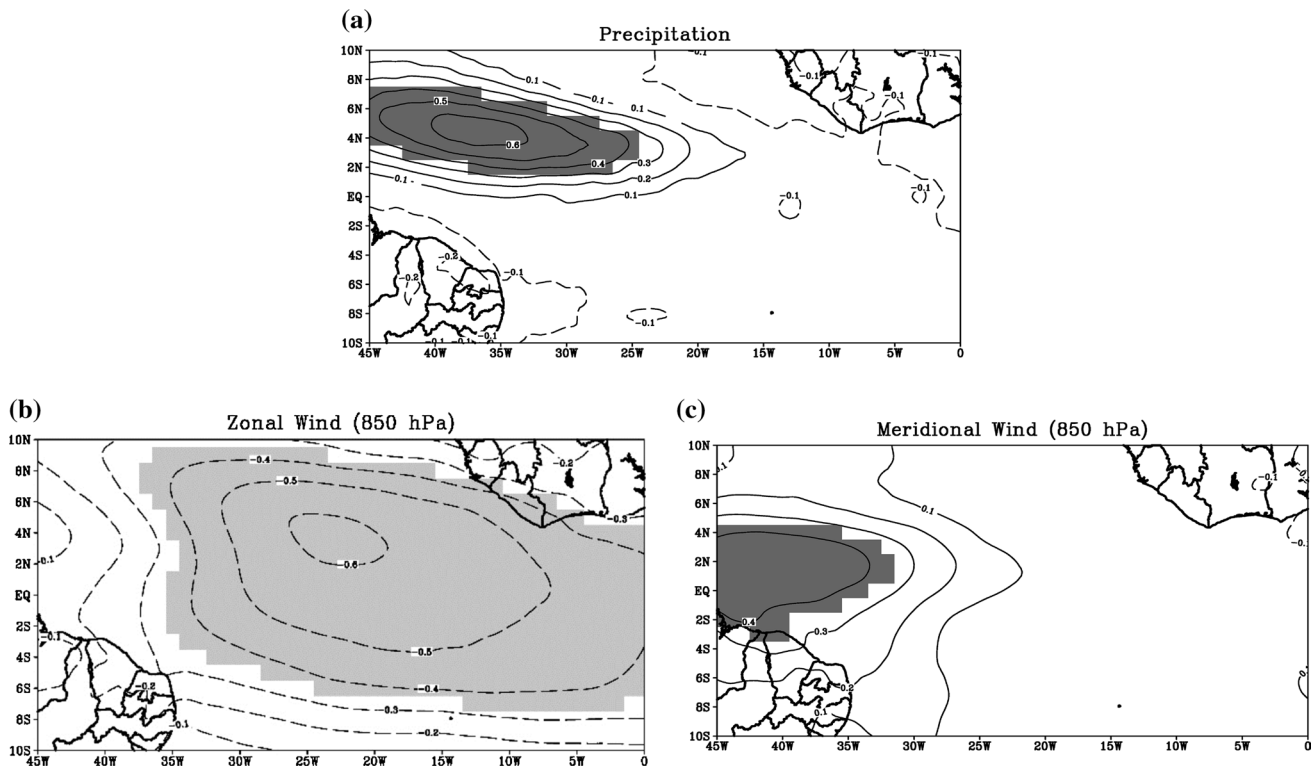

Fig. 1 Pearson linear correlation coefficient (interval of 0.1) between the ITCZi time series and anomalies (annual cycle removed) of **a** precipitation, 850 hPa **b** zonal and **c** meridional wind components. *Continuous* and *dashed lines* represent positive and negative correlation coefficients, respectively. *Shaded areas* in *light* and *dark gray* correspond to regions where negative and positive correlation coefficients are statistically significant at 5 % level, respectively

in the statistical test (Student's t test) of significance of correlations is assumed to be equal to the number of seasons. Although all variables included in the index exhibit lag −1 autocorrelation of <0.5 over the CEOF domain (not shown), this relatively restrictive criterion to estimate the degree of freedom minimizes the influence of interannual variability that could eventually inflate the significance of the correlations. Thus, CEOF-1 is associated with enhanced precipitation over tropical Atlantic west of 20°W, with maximum correlation around 5°N (Fig. 1a). This pattern is associated with easterly wind anomalies dominating the Equatorial Atlantic (Fig. 1b) with high magnitudes east of the region where maximum correlation with precipitation is observed. These features are accompanied by southerly wind anomalies over the western equatorial Atlantic extending from the north coast of South America approximately to 5°N (Fig. 1c). Therefore, CEOF-1 represents the dominant pattern of variability of the Atlantic ITCZ around its climatological position ~5°N (Waliser and Gautier 1993). Moreover,

the CEOF-patterns indicate that the intensification of the A-ITCZ, as expected, is associated with the strengthening of the trade winds and their convergence around the equatorial Atlantic. Given the close correspondence between CEOF-1 and the A-ITCZ we will use CEOF-1 time coefficient as a multivariate index for the A-ITCZ (hereafter ITCZi for simplification).

3.1 Temporal characteristics of the ITCZi

Figure 2 exemplifies the time series of the ITCZi for the period 1979–1982. Positive (negative) and high values of the index indicate pentads during which we observe intense (weak) trade winds leading to strong (weak) convergence of low level winds over the West Atlantic and enhanced (suppressed) precipitation over the West Equatorial Atlantic, characterizing intense (weak) A-ITCZ. It also indicates that the A-ITCZ exhibits variations on intraseasonal-to-interannual time-scales.

To illustrate these issues further, we calculate the power spectrum of the ITCZi (Fig. 3). The raw spectrum was smoothed with 9 points moving average following Chatfield (1996), and zoomed (between 10 and 100 days) in Fig. 3b to emphasize the intraseasonal band. The ITCZi exhibits statistically significant peaks at low frequency (around 5 years) (likely related to the influence of the El Niño-Southern Oscillation-ENSO) (Fig. 3a), between 36 and 40 pentads (likely associated with the A-ITCZ semi-annual cycle); and on intraseasonal timescales approximately between or 3–4 pentads (or 15–20 days, Fig. 3b). We recall that the annual cycle was removed from all variables before performing the CEOF which explains the absence of statistically significant peaks around 1 year. The present study is concerned with intraseasonal variation of the Atlantic ITCZ and all other fluctuations in the convergence zone are beyond the scope of this article.
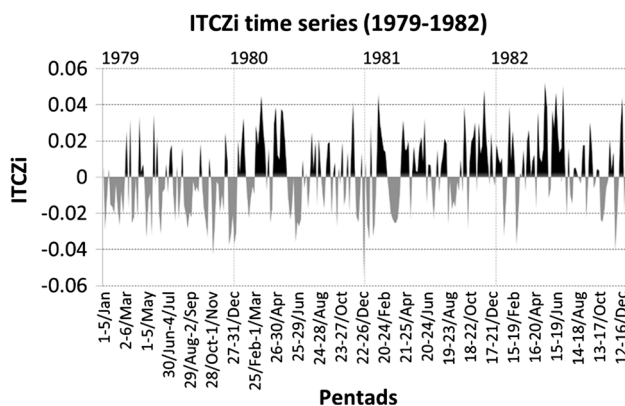

Fig. 2 Example of ITCZi time series for the period of 1979–1982. Negative and positive values are in *gray* and *black*, respectively
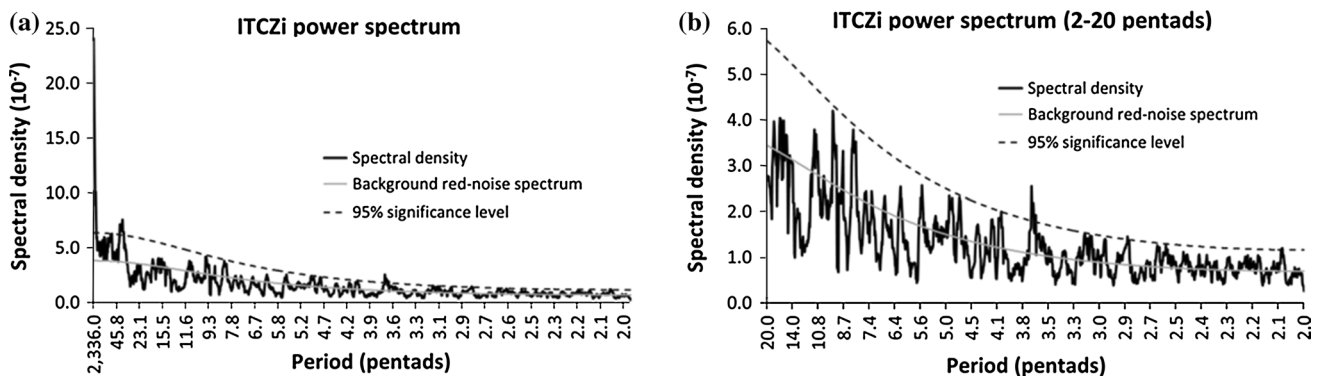

Fig. 3 **a** ITCZi power spectrum of the ITCZi (1979–2010) (*black continuous line*). The *gray line* is the background red-noise spectrum and the *black dashed line* is the 95 % significance level. **b** Magnifies the spectrum in (**a**) for periods between 2 and 20 pentads (10–100 days)

The significant spectral peaks between 10 and 20 days in the ITCZi power spectrum are consistent with the intraseasonal peak obtained in Uvo and Nobre (1989) for the A-ITCZ around 35°W, 40°W and 45°W and has support in a few other studies. For instance, during the austral summer (November–March, NDJFM) observational analyses (Liebmann et al. 1999; Nogués-Paegle et al. 2000; Carvalho et al. 2011) evidenced that intraseasonal variations in the South Atlantic Convergence Zone (SACZ) on timescales roughly between 10 and 20 days are associated with a wave train propagating from the extratropics to the tropics across the South Atlantic Ocean. This wave train modulates convective activity from the subtropics of the Southern Hemisphere to equatorial latitudes and could be source of subseasonal variability in the A-ITCZ. During the austral winter (May–September, MJJAS) the monsoon over West Africa exhibits variations on intraseasonal time-scales that have been associated with significant changes in rainfall and circulation in equatorial latitudes. These phenomena are likely associated with changes in the characteristics of the A-ITCZ, including the quasi-biweekly oscillation in the easterly winds (Grodsky and Carton 2001; Mounier et al. 2008) and respective intraseasonal variability in precipitation and circulation regimes (Janicot and Sultan 2001; Sultan et al. 2003; Maloney and Shaman 2008).

Several sensitivity tests were performed to evaluate the best CEOF domain and set of variables suitable to identify the characteristics of the A-ITCZ (not shown). The decision on the number and type of variables and the best domain for this analysis was based on the ability of the index to identify the most important and well known characteristics of the A-ITCZ such as maximum precipitation band around 5°N and the convergence of the trade winds. Large domains over the Atlantic do not significantly change the spatial correlations discussed here, but result in much less explanation

of the variance by CEOF-1. As we pointed out before, we are also interested in the realistic spectral variance of the index. The set of variables used in this study provides the most reliable results regarding both the spatio-temporal characteristics of the A-ITCZ and its spectral variance.

4 Intraseasonal variability of the A-ITCZ

This section focuses on characterizing the intraseasonal variability of the A-ITCZ. For this purpose the ITCZi was band-pass filtered with a Fast Fourier Transform (FFT) based filter (e.g., Chatfield 1996) to retain frequencies corresponding to 10–70 days. The filtered ITCZi will hereafter be referred to as $ITCZ_{10-70}$. Intense (weak) intraseasonal events were identified when the $ITCZ_{10-70}$ was above its 75th (below its 25th) percentile. We investigated separately events that occurred during the austral summer (November–March, NDJFM) and the austral winter (May–September, MJJAS). For simplification, the two seasons are henceforth referred to as 'summer' and 'winter', respectively. Notice that the percentiles were calculated for each season separately as the variance of the index depends on the season. We considered as independent events those occurrences that were at least 2 pentads apart (~10 days) from each other, consistent with the scale of the phenomenon (intraseasonal). We defined as "persistence" of the event the number of consecutive pentads that exhibited $ITCZ_{10-70}$ above its 75th (below its 25th) percentile.

Figure 4 shows the interannual variability in the number of weak and intense $ITCZ_{10-70}$ events from 1979 to 2010. During the summer (Fig. 4a), we observe on average 5 intense and weak events a year with standard deviation around ±1 event. The average number of events is approximately the same during the winter (Fig. 4b). Furthermore,
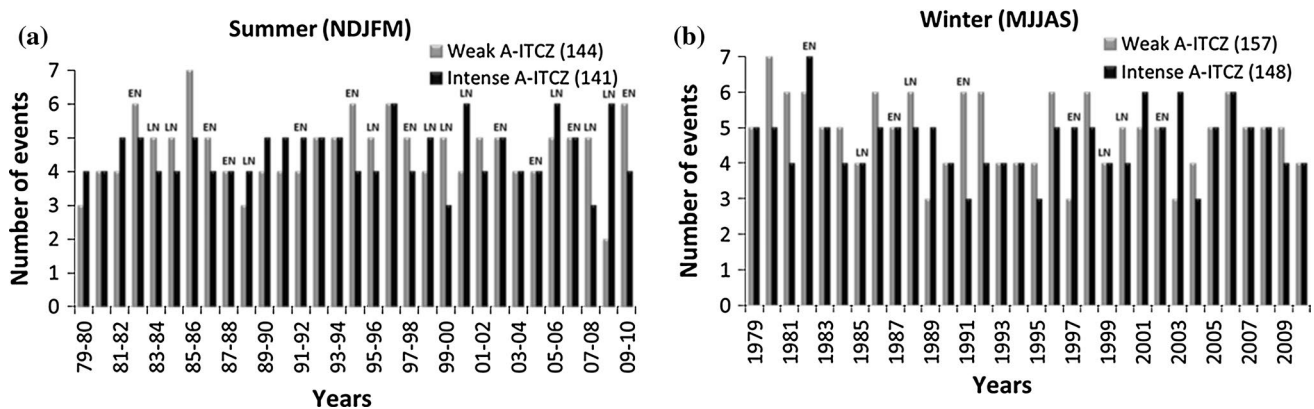

Fig. 4 Interannual variability of the number of intraseasonal events of weak and intense A-ITCZ for the period of 1979–2010 for austral **a** summer and **b** winter. The *numbers in parenthesis* represent the total number of independent events of weak and intense $ITCZ_{10-70}$. The labels EN and LN indicate years of moderate to strong El Niño and La Niña in the period, respectively
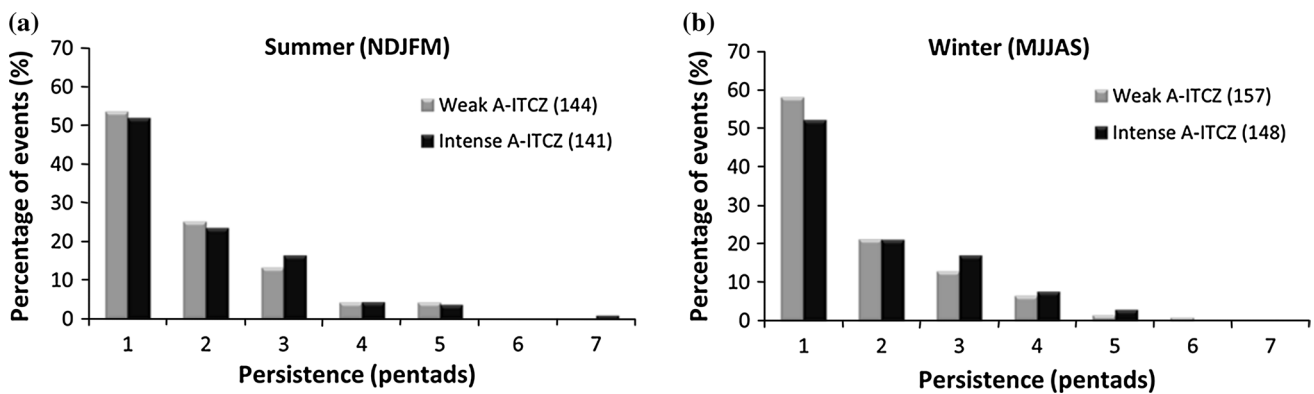
(a)

(b)

Fig. 5 Percentage of intraseasonal events of weak and intense ITCZ$_{10-70}$ versus persistence in pentads for the period of 1979–2010 for austral **a** summer and **b** winter. The *numbers in parenthesis* in the captions represent the total number of independent events of weak and intense ITCZ$_{10-70}$

the number of week and intense events per season is similar in both seasons. In the summer, the maximum number of intense (weak) events during the period of this analysis is equal 6 (7). This methodology identified 144 (157) weak ITCZ$_{10-70}$ events and 141 (148) intense ITCZ$_{10-70}$ events in the summer (winter) during 1979–2010. No statistically significant trend is observed in the number of events during the studied period. Furthermore, there is no clear association between the frequency of intraseasonal events and ENSO. These results seem consistent with De Souza et al. (2005) who showed that wet and dry periods over Northeast Brazil and East Amazon (largely modulated by the A-ITCZ) on intraseasonal time-scales exhibit a weak relationship with ENSO and with the inter-hemispheric gradient of sea surface temperature (SST) over the Atlantic.

Approximately 50 % of all intense and weak events have duration of about 1 pentad during the summer (Fig. 5a) and winter (Fig. 5b) and <5 % of all events last more than 4 pentads in the analyzed period. The maximum duration of intense ITCZ$_{10-70}$ is 7 pentads and this event happened in the summer. The maximum duration of weak ITCZ$_{10-70}$ is 6 pentads and this event occurred in the winter. There is no clear relationship between the intensity of the event (based on the ITCZ$_{10-70}$ index) and the duration of the event (not shown). We emphasize that the duration of an 'event' depends on the threshold of intensity or the percentiles used to select events based on the ITCZ$_{10-70}$.
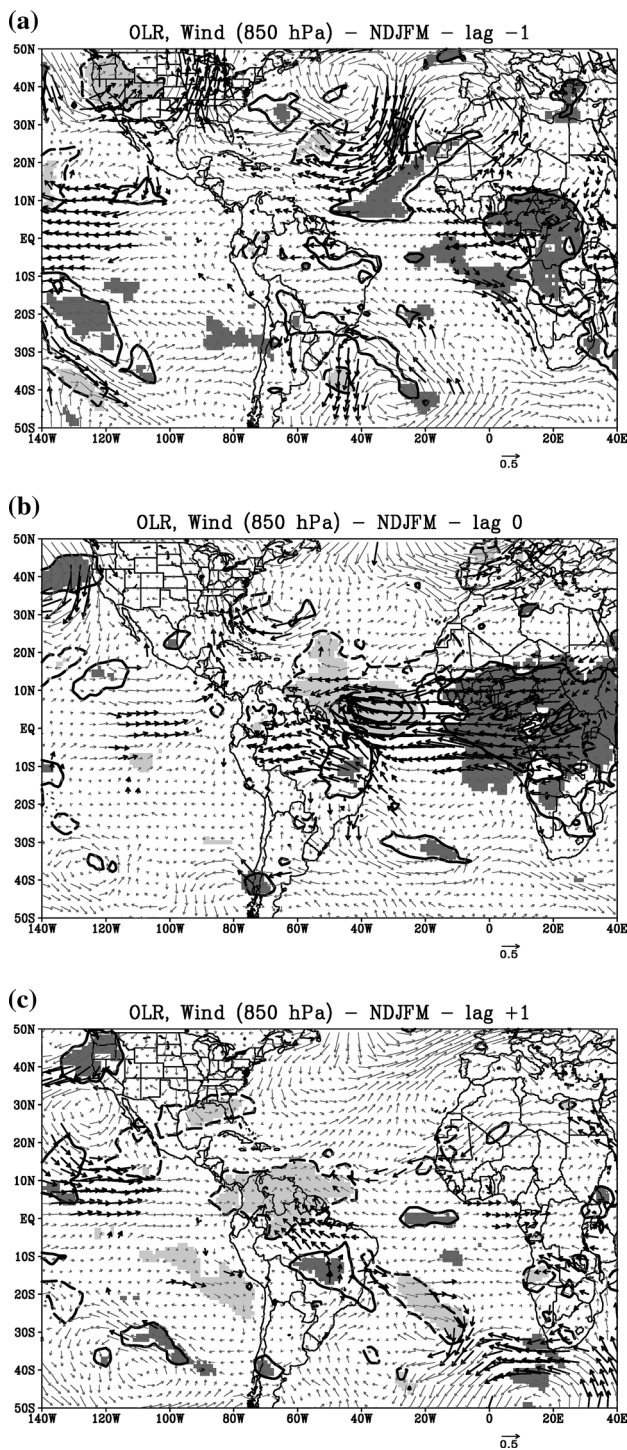
4.1 Mechanisms: austral summer

This section investigates the mechanisms associated with ITCZ$_{10-70}$ by performing lag composites around the events selected in the previous section. All atmospheric variables are band-pass filtered on intraseasonal time-scales (10–70 days) using the same FFT filter. Lag composites are performed from one pentad prior to the event to one pentad after the event, consistent with the median duration of events (between 1 and 2 pentads, see Fig. 5). No spatially coherent and statistically significant anomalies are observed before and after the analyzed period (−1 to +1 pentad) (not shown). Patterns of anomalies observed for intense and weak ITCZ$_{10-70}$ are similar but with opposite sign in the tropics. Here we focus only on composites calculated for intense ITCZ$_{10-70}$ events.

One pentad prior to the intense event (lag −1, Fig. 6a) intraseasonal easterly wind anomalies intensify at low levels of the troposphere (850 hPa) over tropical North Atlantic. These anomalies in the trade winds are associated with the strengthening of the North Atlantic anticyclone. Positive OLR anomalies near eastern equatorial Atlantic are consistent with the intensification of subsidence associated with the strengthening of the anticyclone. We can also observe the concomitant presence of a pair of troughs, one located in the west coast of the United States and the other one over northwestern Africa, and also a ridge over northern tropical Africa (Fig. 6a). These features indicate that anomalous North Atlantic anticyclone is part of a Rossby wave train on intraseasonal time-scales modulating the NH circulation. However, the Rossby wave trains are better characterized when observing circulation and geopotential in 200 hPa. For instance, Fig. 7a shows alternating intraseasonal anomalies of the meridional component of the wind in 200 hPa exhibiting an arc-like feature with poleward orientation on the west side and equatorward orientation on the east side of the arc reinforcing the hypothesis of the organization of a Rossby wave train (e.g., Hoskins and Karoly 1981).

The vertical structure of the wave train can be observed from composites of the intraseasonal anomalies of the 200 hPa geopotential height and circulation (Fig. 8). Cyclonic (anticyclonic) wind anomalies in 850 hPa (Fig. 6a) vertically aligned with an anomalous trough

(a)

(b)

(c)

◀**Fig. 6** Lag composites of intraseasonal (10–70 days) anomalies of OLR (*contours*) and 850 hPa wind (*vectors*) (m s^{-1}) for the intense ITCZ$_{10-70}$ for austral summer (NDJFM). Thick vectors correspond to statistically significant anomalies at 5 % level. Statistically significant wind anomalies are considered where at least one of the components of the wind (zonal and/or meridional) is statistically significant. *Dashed* and *continuous contours* represent negative (minimum contour of -1.5 W m^{-2}) and positive OLR anomalies (minimum contour of 1.5 W m^{-2}), respectively, with an interval of 2.5 W m^{-2}. *Shaded areas* in *light* (*dark*) *gray* correspond to regions where the negative (positive) OLR anomalies are statistically significant at 5 % level. Lags correspond to pentads: **a** lag -1, **b** lag -0, **c** lag $+1$ pentads

(ridge) in 200 hPa (Fig. 8a) and respective cyclonic (anticyclonic) anomalous circulation in 200 hPa (Fig. 9a) evidence a barotropic structure, which supports the presence of a Rossby wave. These features characterize the tropical-extratropical teleconnection patterns discussed in Hoskins and Karoly (1981) with horizontal structure described in Wallace and Gutzler (1981). These authors point out that the wave patterns are in general characterized by several

centers of action in mid and upper levels of the atmosphere but exhibit one or two well defined centers of action near the surface. Additionally, the intensification of the trade winds over the North Atlantic and West Africa for lag -1 (Fig. 6a) is associated with positive geopotential anomalies (Fig. 8a) and anticyclonic circulation (Fig. 9a) in upper levels, which is consistent with the equivalent barotropic vertical structure of the Rossby wave (e.g., Hoskins and Karoly 1981).

At the pentad of the event (lag -0) statistically significant easterly wind anomalies in the low troposphere (Fig. 6b) dominate over tropical Atlantic and West Africa and clearly indicate the intensification of the trade winds in low latitudes. The enhancement of the A-ITCZ can be identified from negative OLR intraseasonal anomalies (~-6.5 W m^{-2}) which are associated with anomalous convergence of trade winds over the west equatorial Atlantic. The strengthening of the easterly winds inhibits the transport of moisture from the ocean toward tropical Africa and further suppresses convection over tropical Western Africa, which can be identified from positive OLR anomalies (Fig. 6b). Easterly wind anomalies are also observed over tropical South America and are related to suppression of convection over this region, which typically occurs during the summer monsoon season (Carvalho et al. 2002, 2004; Jones and Carvalho 2002).

Moreover, intraseasonal anomalies in the meridional winds in 200 hPa for lag -0 (Fig. 7b) indicate that the Rossby wave propagates eastward across the Atlantic and bifurcates following two main paths (black arrows in Fig. 7b): one in midlatitudes toward Eurasia and a second one following an arc-like path toward the equator (e.g., Hoskins and Karoly 1981; Webster and Holton 1982), which is consistent with the "North America-Atlantic" wave guide identified in Hsu and Lin (1992). Upper level divergence collocated with negative OLR anomalies (Fig. 6b) is evident from the anomalies of the 200 hPa meridional winds (Fig. 7b) in agreement with the intensification of the ITCZ$_{10-70}$. Therefore, the ITCZ$_{10-70}$ intense events are associated with enhanced trade winds forced by the intensification of the anticyclonic circulation over the North Atlantic. These changes in circulation result in strong
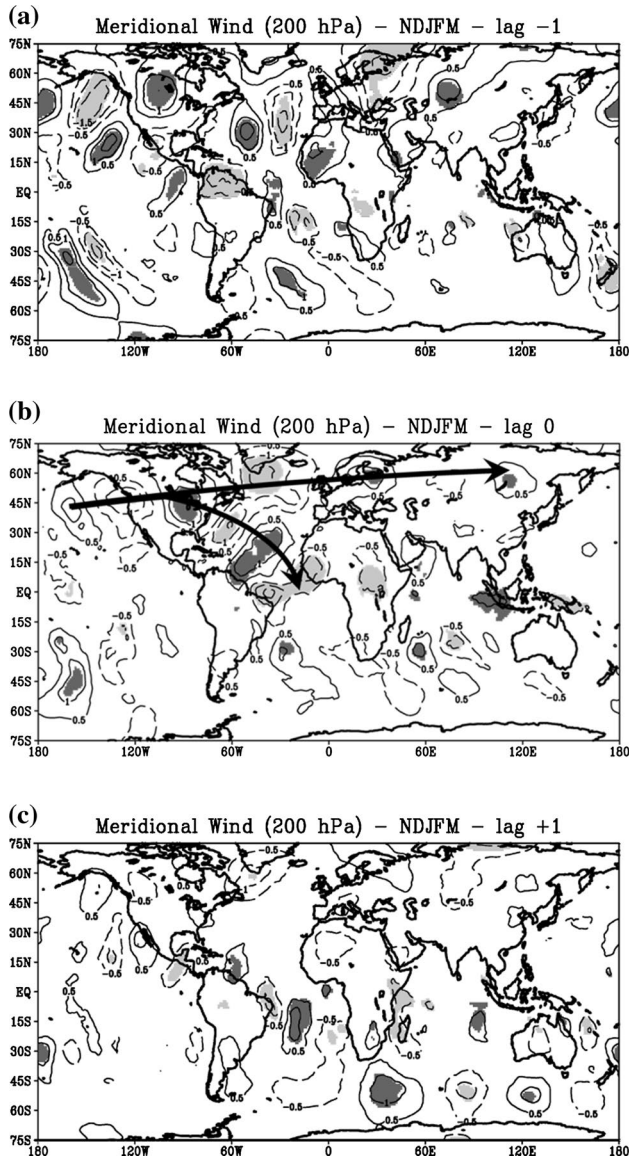
(a)

(b)

(c)

Fig. 7 Lag composites of intraseasonal (10–70 days) anomalies of 200 hPa meridional component of the wind for the intense ITCZ$_{10-70}$ for austral summer (NDJFM). *Dashed* and *continuous contours* represent negative (minimum contour of -0.5 m s^{-1}) and positive anomalies (minimum contour of 0.5 m s^{-1}), respectively, with an interval of 0.5 m s^{-1}. *Shaded areas* in *light* (*dark*) *gray* correspond to regions where the negative (positive) anomalies are statistically significant at 5 % level: **a** lag -1, **b** lag -0, **c** lag $+1$ pentads. *Black arrows* in (**b**) indicate the main midlatitude wave train paths

low-level convergence coupled to intense upper-level divergence and enhanced convection in the ITCZ$_{10-70}$ (Fig. 9b). This vertical coupling suggests a barotropic-to-baroclinic transition of the wave pattern near the equator at lag -0, a dynamical response due to intensified convective activity.
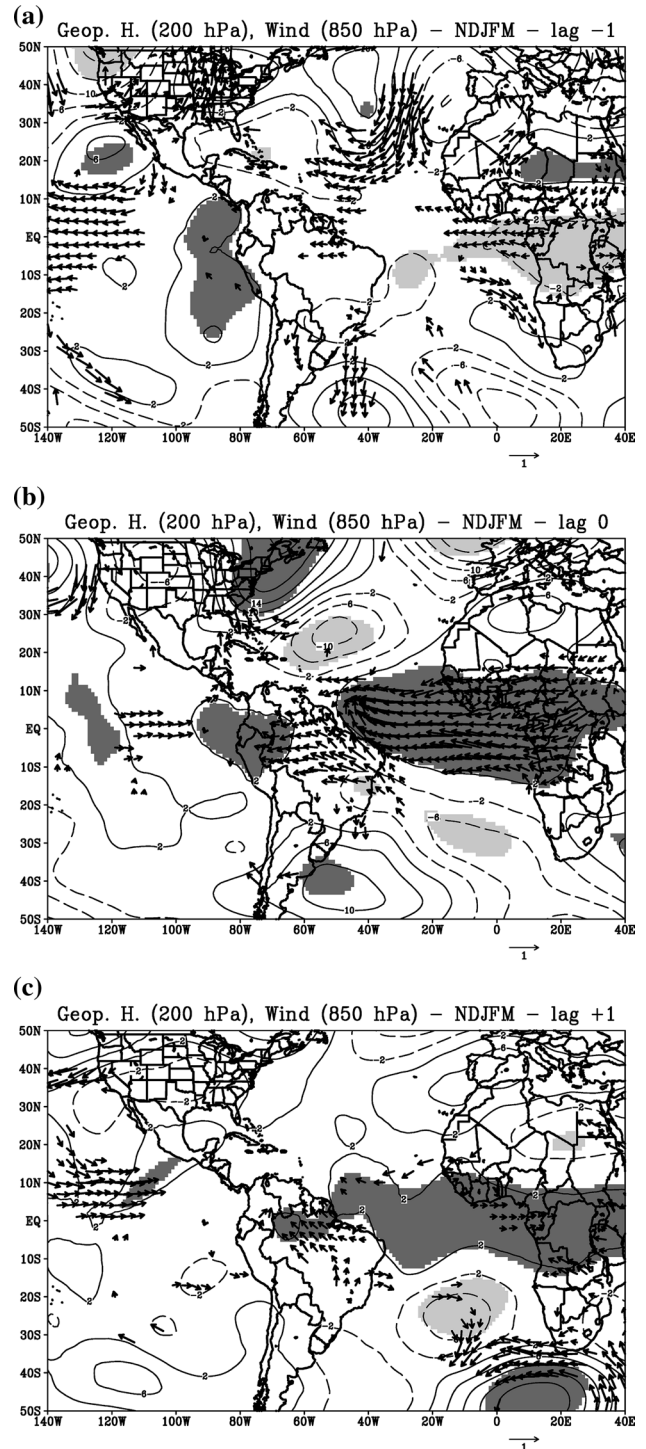
(a)

(b)

(c)

Fig. 8 As in Fig. 6 but for 200 hPa geopotential height (*contours*) and 850 hPa wind (*vectors*) (m s^{-1}). Only statistically significant wind anomalies at 5 % level are plotted. *Dashed* and *continuous contours* represent negative (minimum contour of -2 m) and positive anomalies (minimum contour of 2 m) of geopotential height, respectively, with an interval of 4 m: **a** lag -1, **b** lag -0, **c** lag $+1$ pentads
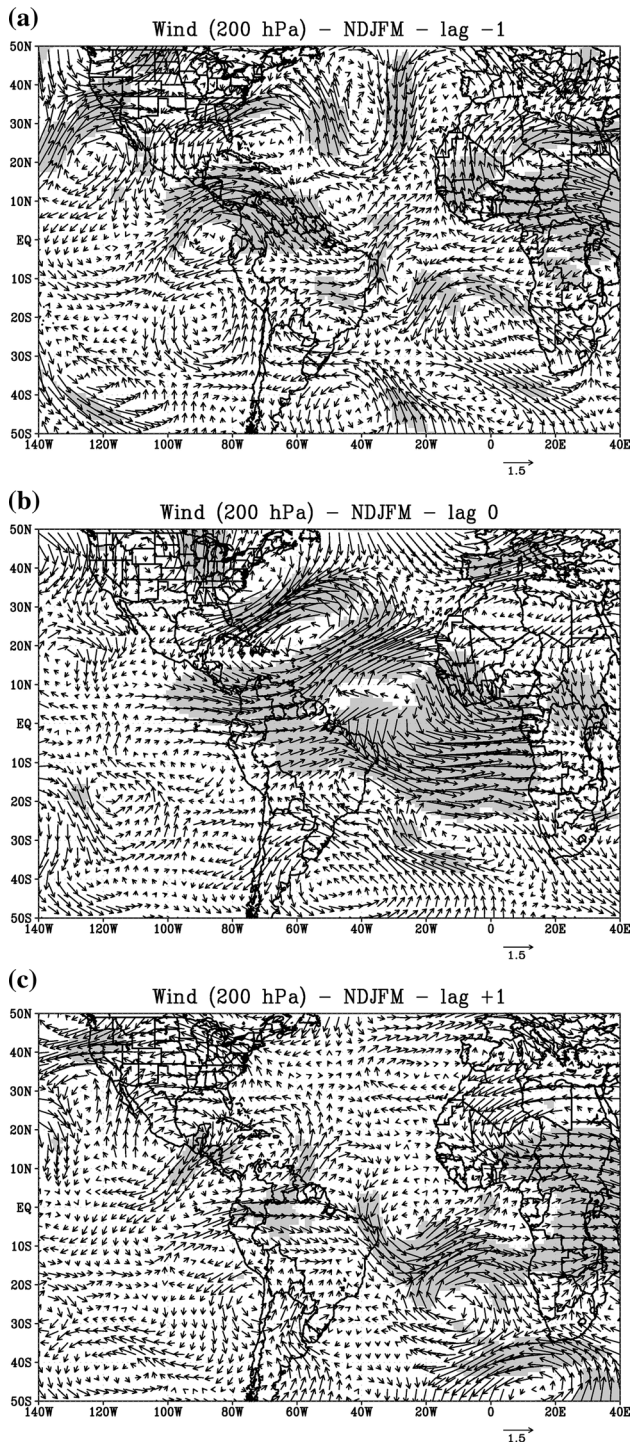
(a)

Wind (200 hPa) – NDJFM – lag −1

(b)

Wind (200 hPa) – NDJFM – lag 0

(c)

Wind (200 hPa) – NDJFM – lag +1

Fig. 9 Lag composites of intraseasonal (10–70 days) anomalies of 200 hPa winds (m s^{-1}) for the intense ITCZ$_{10-70}$ for austral summer (NDJFM). *Shaded areas* correspond to regions where anomalies are statistically significant at 5 % level: **a** lag −1, **b** lag −0, **c** lag +1 pentads

One pentad after the ITCZ$_{10-70}$ intense event (lag +1, Fig. 6c) the pattern of easterly anomalies weakens over eastern equatorial Atlantic, while negative OLR anomalies (weaker than for lag −0) persist over northern South America and western equatorial Atlantic. Suppression of convection also persists over tropical South America. Additionally, we hypothesize that there is cross-equatorial propagation of the wave train toward the Southern Hemisphere for lag +1. Negative OLR anomalies with northwest-southeast orientation observed extending from tropical to subtropical South Atlantic and resembling a frontal system (Fig. 6c) evidences the wave train in the Southern Hemisphere. The enhancement of the intraseasonal geopotential anomalies (Fig. 8c) along with the wave-like pattern shown in 200 hPa winds (Fig. 9c) in the Southern Hemisphere during lag +1 corroborate with this hypothesis. Mechanisms explaining cross-equatorial propagation have been discussed in Webster and Holton (1982), Tomas and Webster (1994), Ji et al. (2014), among others.

Ji et al. (2014) investigated the mechanisms that control the inter-hemispheric teleconnections from tropical heat sources using an intermediate complexity model. They illustrate the inter-hemispheric teleconnection process with a heat source placed over the Atlantic warm pool that directly excites a baroclinic response that spreads across the equator. They postulate that three processes involving baroclinic–barotropic interactions force a cross-equatorial barotropic Rossby wave response: shear advection, surface drag, and vertical advection. In the present case, Rossby waves (which exhibit a barotropic structure) force convection in the A-ITCZ near equatorial latitudes and when convection is fully developed the atmosphere exhibits a baroclinic profile (barotropic-to-baroclinic transition). Similarly, the enhancement of convection in the A-ITCZ could excite cross-equatorial barotropic Rossby wave response, explaining the observed wave patterns in the Southern Hemisphere for lag +1. Strong westerly anomalies in 200 hPa (Fig. 9) collocated with strong easterly anomalies in 850 hPa (Fig. 6) over tropical South America and western South Atlantic for all lags, suggest that the shear advection is likely an important process in this case. In addition, with a nonlinear model based on shallow water equations, Webster and Holton (1982) showed that large scale disturbances that propagate in one hemisphere can influence the other hemisphere in the presence of westelies ("westerly duct") in some equatorial region. Moreover, Tomas and Webster (1994) showed that fluctuations with periods of 6–30 days in eastern Pacific can propagate from NH extratropics, cross the equator and continue propagating to Southern Hemisphere. They highlight that this result is in agreement with the hypothesis that westerlies in the tropics act as a "duct" allowing inter-hemispheric propagation of extratropical Rossby waves during boreal winter. Upper-level westerlies dominate the equatorial Atlantic from lag −1 to lag +1 (not shown) and thus create the 'westerly duct' for the cross-equatorial propagation suggested by the wave patterns in Southern Hemisphere at lag +1.
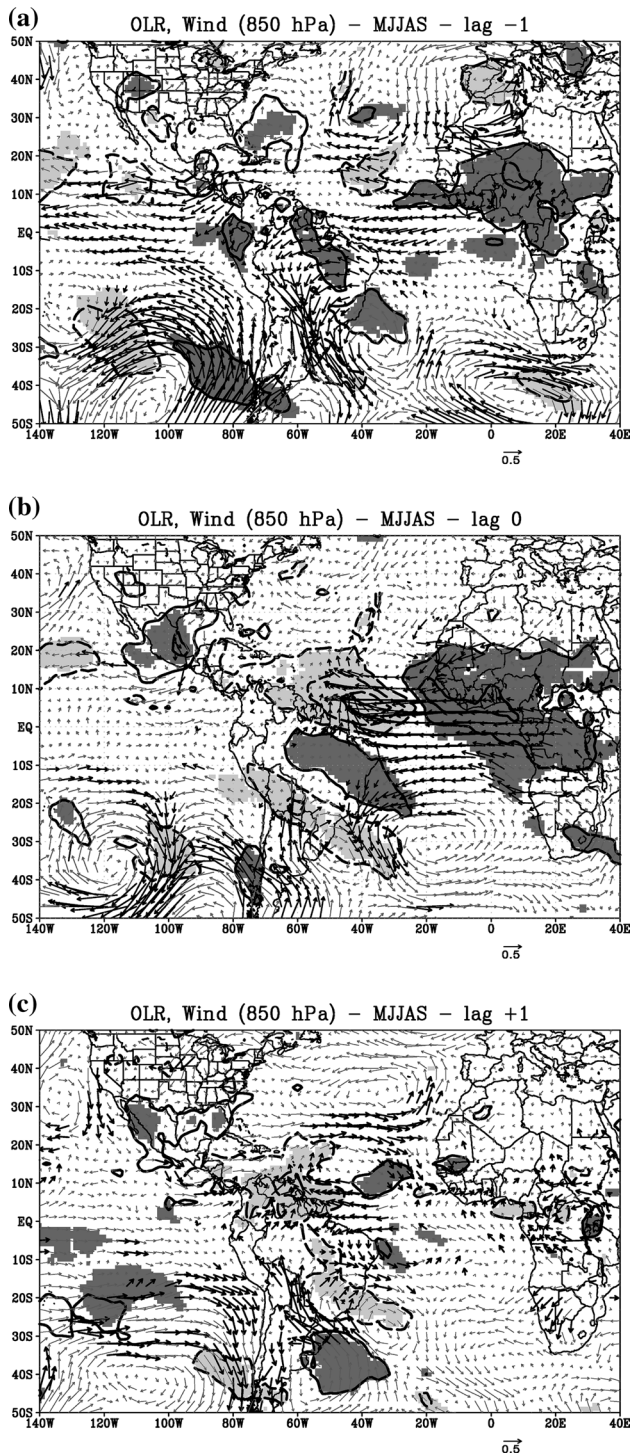
Fig. 10 As Fig. 6 but for austral winter

4.2 Mechanisms: austral winter

Analogous to the ITCZ$_{10–70}$ events during the austral summer, weak and intense intraseasonal events during the winter exhibit similar but opposite characteristics over the equatorial Atlantic and this section will discuss only intense
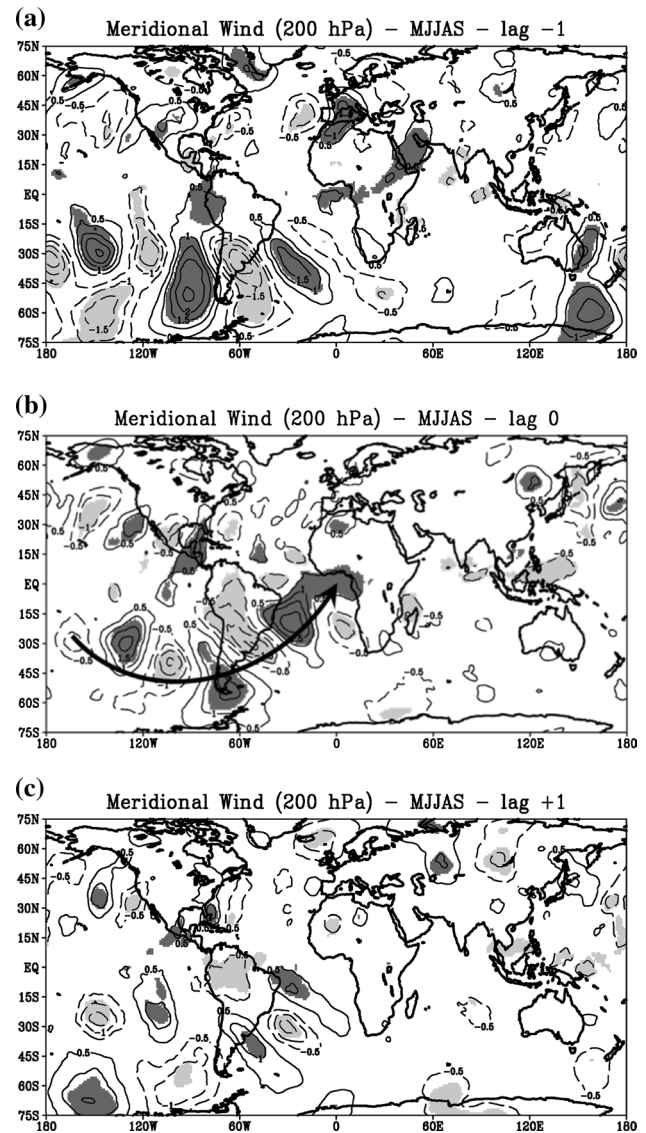

Fig. 11 As Fig. 7 but for austral winter

events. As we will demonstrate, these events are largely modulated by atmospheric disturbances that develop in the winter hemisphere (in this case, the Southern Hemisphere).

One pentad before the event (lag −1, Fig. 10a) easterly wind anomalies dominate tropical and equatorial Atlantic, tropical South America and Western Africa indicating the strengthening of the trade winds. As discussed for the austral summer, these anomalies weaken moisture transport toward Western Africa resulting in suppression of convective activity in this region as indicated by positive OLR anomalies (Fig. 10a). Likewise, easterly anomalies and suppressed convection are also observed over tropical South America due to the westward shifting of the Atlantic anticyclone and consequent intensification of subsidence over the continent. At this stage, enhanced convective

activity over the tropical Atlantic is restricted to an area that extends roughly between 10°–20°N and 30°–40°W. Alternating anomalous cyclonic and anticyclonic circulation centers at 850 hPa characterize the presence of a midlatitude wave train in the Southern Hemisphere. The 200 hPa meridional wind anomalies (Fig. 11a) are also consistent with the presence of a well-developed wave train in the Southern Hemisphere with zonal wave number 3–4 resembling the Pacific-South American (PSA) teleconnection pattern (Mo and Ghil 1987). This Rossby wave emanates from the Western South Pacific, following the wave guide associated with the subtropical jet of the Southern Hemisphere and the preferential propagation path toward tropical South Atlantic discussed in Hoskins and Ambrizzi (1993).

Figure 12a indicates the vertical structure of the Rossby wave train for lag −1 and shows that the anomalous ridge (trough) identified with positive (negative) geopotential height anomalies in upper levels of the Southern Hemisphere is nearly vertically aligned with the anomalous and statistically significant anticyclonic (cyclonic) circulation at low levels. This vertical profile of circulation and geopotential characterizes the equivalent barotropic structure linked to the Rossby wave dynamics. The anomalous cyclonic circulation in 200 hPa over Argentina and anticyclonic circulation near the southern coast of Brazil (Fig. 13a) is consistent with the positive phase of the first PSA mode (Mo and Higgins 1998).

The strengthening of the trade winds over eastern South Atlantic at lag −1 (Fig. 10a) is associated with the intensification of anomalous anticyclonic circulation near the southeast coast of Brazil, which is part of the wave train feature. Notice that the wave train exhibits a nearly barotropic structure over the Southern Pacific but a poleward and westward tilt with height as it approaches the western South Atlantic (Fig. 12a). The transition to a more baroclinic structure as the wave train moves equatorward has been observed before in association with the development of the SACZ during the summer (Liebmann et al. 1999). In addition, the 200 hPa geopotential height (Fig. 12a) and 200 hPa wind (Fig. 13a) anomalies indicate the presence of a trough (ridge) in the west (east) coast of the U.S. These features are better characterized in upper level circulation and geopotential rather than low-level winds and OLR anomalies (compare Figs. 13a, 12a with Fig. 10a). A plausible explanation is the relatively weak support for well-developed frontal bands in the NH during the boreal summer.

At the pentad of the event (lag −0, Fig. 10b) we observe the strengthening of the South Atlantic anticyclonic circulation in low levels relative to lag −1. The 200 hPa meridional winds (Fig. 11b), geopotential (Fig. 12b) and circulation (Fig. 13b) anomalies characterize the Rossby
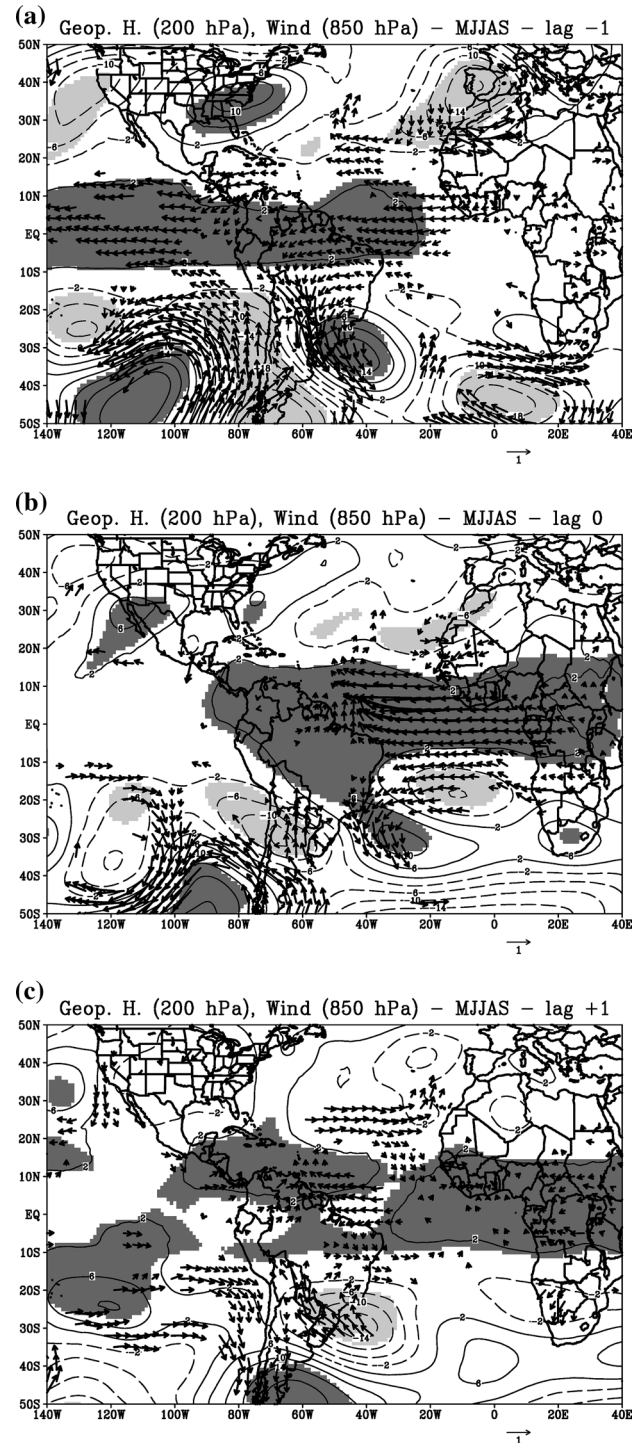

Fig. 12 As Fig. 8 but for austral winter

wave pattern in the Southern Hemisphere, whose main path is indicated by a black arrow in Fig. 11b. Analogous to the austral summer, the strengthening of Atlantic anticyclone results in intensified low-level convergence of the trade winds near the equator that enhance convection in the A-ITCZ, as indicated by negative OLR anomalies
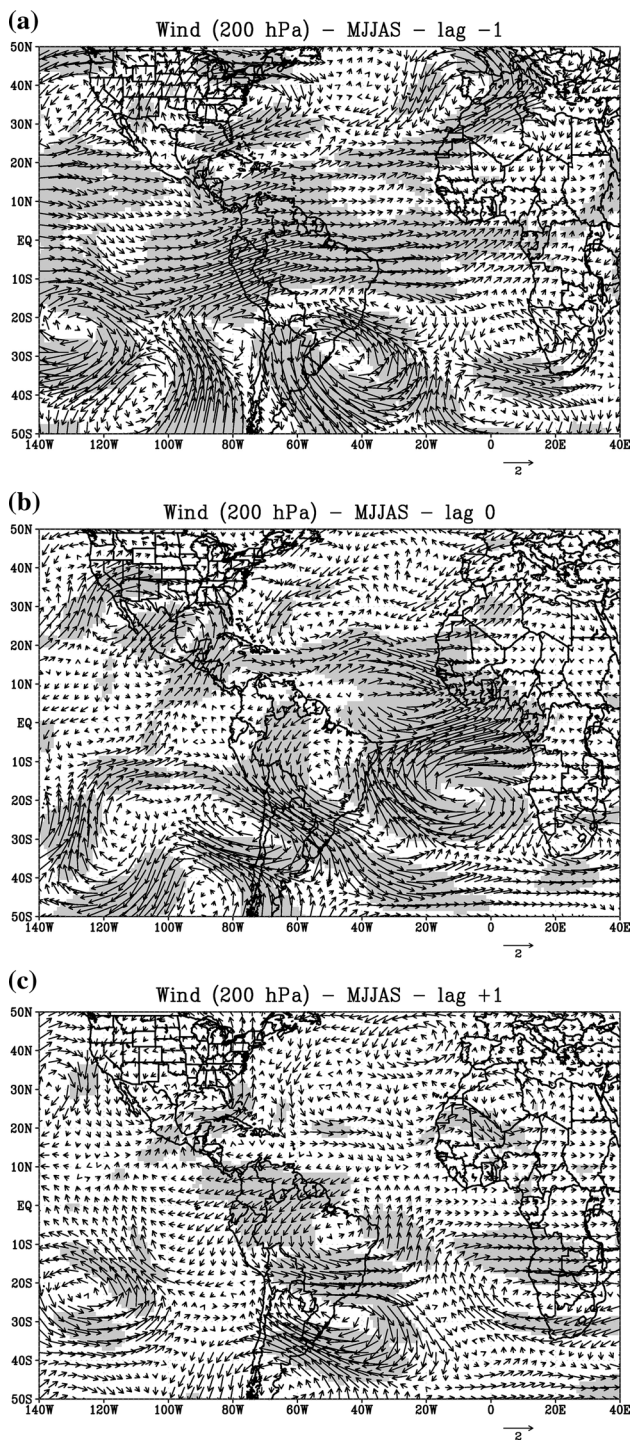
(a)

(b)

(c)

Fig. 13 As Fig. 9 but for austral winter

of about -6.5 W m^{-2}. The area with convective activity extends now over coastal areas of northern South America. Meanwhile, the strengthening of the South Atlantic anticyclone results in easterly wind anomalies and strong subsidence over eastern Brazil causing suppression of convective activity in this region (Fig. 10b). A convective band

develops poleward of the intensified northwesterly winds indicating the development of a frontal system extending from the Andes toward La Plata Basin and western South Atlantic. These combined features characterize the alternating pattern of circulation and convection associated with the midlatitude wave train. Moreover, the nearly baroclinic structure associated with the intensification of convection in the ITCZ$_{10-70}$ is evident from the anomalous westerly winds observed near the Equator at lag -0 (Fig. 13b). The enhancement of convective activity intensifies the cross-equatorial transport near the area with maximum convection, as indicated by southerly wind anomalies where convection is maxima (Fig. 12b).

It is worth noting that the anomalous circulation in low latitudes associated with intensified ITCZ$_{10-70}$ is typical of break phases in the sub-Saharan African monsoon (e.g., Sultan et al. 2003; Maloney and Shaman 2008). Thus, a zonal (east–west) dipole characterized by enhanced convection west of 20°W and suppression east of 20°W is evident over the Equatorial Atlantic (Fig. 10b). This stage characterizes the peak of convection in the ITCZ$_{10-70}$.

One pentad later (lag $+1$), easterly anomalies weaken and convective anomalies in the ITCZ$_{10-70}$ move westward over the Caribbean, affecting Venezuela, Colombia and equatorial Central America (Fig. 10c). These changes are also observed along with the weakening of the easterly anomalies over Africa and South America. The South Atlantic anticyclone weakens and cyclonic anomalies replace the anticyclonic anomalies over subtropical South Atlantic. Consequently, the frontal band observed in the subtropics of South America at lag -0 moves equatorward characterizing a new phase of the midlatitude wave train. The upper level wind divergence over the ITCZ$_{10-70}$ significantly weakens (Fig. 13c) indicating the weakening of the dynamical support for enhanced convection forced by the Rossby wave train near the Equator.

5 Relationships with the MJO

The power spectrum (Fig. 3) shows that ITCZi exhibits variability on scales ranging from 10 to 70 days. The motivation for this investigation is the association of the MJO with Rossby wave response that affects midlatitudes of both hemispheres on intraseasonal time-scales (Knutson and Weickmann 1987; Hendon and Salby 1994; Liebmann et al. 1999; Carvalho et al. 2004; Zhang 2005; Cunningham and Cavalcanti 2006; Becker et al. 2011).

Here we objectively examine the relationships between MJO and ITCZ$_{10-70}$ by identifying MJO events using a multivariate index based on the methodology discussed in Jones (2009) and summarized as follows. This method uses combined empirical orthogonal function (CEOF)
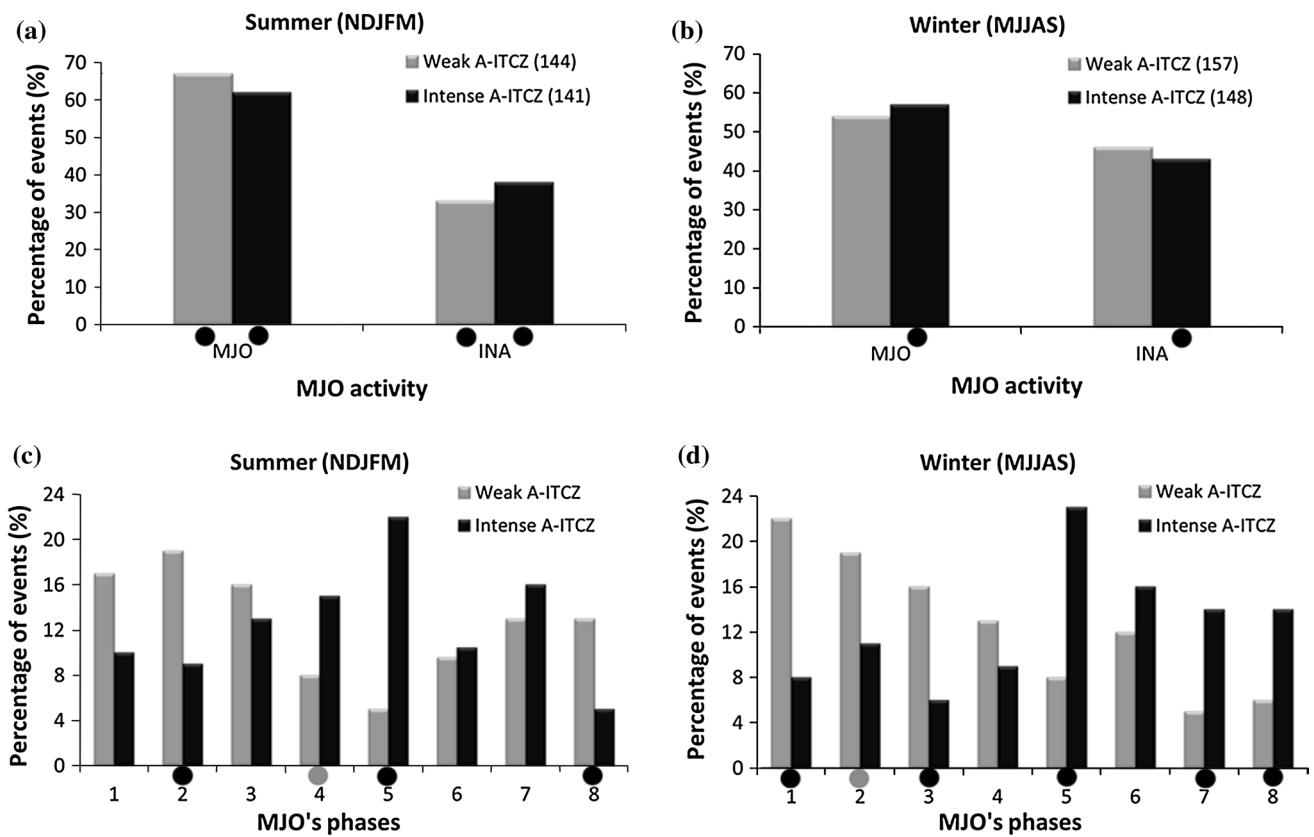
Fig. 14 Percentage of intraseasonal events of weak and intense A-ITCZ that occurred during MJO active (MJO) and inactive (INA) phases for austral **a** summer and **b** winter. The *numbers between parentheses* represent the total number of independent events. Percentage of intraseasonal events that occurred during each MJO phase for austral **c** summer and **d** winter. Percent values in (**c**) and (**d**) are relative to all events that occurred during "active MJO" in each season. *Black* (*gray*) *circles* next to the *horizontal axis* indicate the differences between the proportions are statistically significant at 5 % (10 %) level

performed on CFSR zonal winds in 850 hPa (U850) and 200 hPa (U200) and OLR intraseasonal anomalies (bandpass filtered between 20 and 200 days) and averaged in latitude (15°S–15°N). The first two CEOFs, which account for about 23.8 and 19.5 % of the total variance respectively, are used to represent the MJO. The equatorial structure of the first two CEOFs can be seen in Jones (2009) and Wheeler and Hendon (2004). The phase diagram based on the first two normalized principal components (CEOF-1, CEOF-2) is then used to identify MJO events according to the following criteria: (1) the phase angle between CEOF-1 and CEOF-2 systematically rotates anti-clockwise indicating eastward propagation at least to phase 5 (maritime continent); (2) the amplitude $(CEOF-1^2 + CEOF-2^2)^{0.5}$ is always larger than 0.35; (3) the mean amplitude during the event is larger than 0.9; (4) the entire duration of the event lasts between 30 and 90 days. This method identifies 8 phases of the oscillation as it moves eastward. All MJO events start in phases 1–4, propagate eastward and end in phases 4–8 (i.e., isolated events) or restarted from previous MJO occurrences (i.e., successive events; phase continues from

8 to 1). The condition of "Inactive MJO" (INA) is defined when the criteria 1–4 are not simultaneously satisfied. The phase composite with U200, U850 and OLR anomalies can be assessed in Jones (2009, see Figs. 2–4 in that paper). A thorough review on the index and its applications can be seen in Jones (2009) and Jones and Carvalho (2011, 2012, 2014). In the present study we use the MJO index to identify the frequency of intense and weak $ITCZ_{10-70}$ when the MJO is active and investigate significant dependence of the relative frequency of these events on MJO phases.

During summer (Fig. 14a) about 62 % (67 %) of all intense (weak) $ITCZ_{10-70}$ events occurred when the MJO was active and the differences in proportions with respect to "inactive MJO" are statistically significant at 5 % significance level (see, e.g., Spiegel 1972 for the statistical test for the difference in proportions). During winter (Fig. 14b) the proportion of intense (weak) $ITCZ_{10-70}$ events occurring when the MJO is active is slightly reduced to about 57 % (54 %). Statistical significance in the difference of proportions in winter (at 5 % significance level) is achieved only for intense events.

As the MJO propagates eastward, it modulates circulation throughout the tropical troposphere with patterns that depend on the phase of the oscillation. The distributions of weak and strong events according to the MJO phase during the summer and winter are shown in Fig. 14c, d, respectively. The percent values are relative to all events that occurred during "active MJO". The statistical significance in the difference in proportions between 'weak' and 'intense' $ITCZ_{10-70}$ events for each MJO phase is indicated in the figure (see Fig. 14 caption). Although intense and weak $ITCZ_{10-70}$ events occur in any phase of the MJO, it is clear that the relative frequency of intense and weak $ITCZ_{10-70}$ events varies according to the phase of the oscillation. Intense $ITCZ_{10-70}$ events dominate over weak $ITCZ_{10-70}$ events during phases 5 (at 5 % significance level) and 4 (at 10 % significance level) whereas weak $ITCZ_{10-70}$ events dominate over intense during phases 2 and 8 in the summer (Fig. 14c). In the winter, the frequency of intense events dominates over the frequency of weak events during phases 5, 7 and 8 (at 5 % significance level) whereas the frequency of weak events dominate over intense events during phases 1, 2 and 3 (Fig. 14d). The association between MJO phases and the $ITCZ_{10-70}$ events can be mostly explained by how the oscillation modulates zonal wind anomalies in tropical latitudes. Phases 4–6 are characterized by dominant easterly wind anomalies in the tropics (15°S–15°N) east of the date line, which includes South America, the Caribbean and the Equatorial Atlantic (see Fig. 3 in Jones 2009). Convection associated with the MJO in these phases is prominent west of the date line and moves from the Indian Ocean toward the date line from phases 4–5 (see Fig. 4 in Jones 2009). These phases have also been associated with suppressed convection over tropical South America and Africa, consistent with the lag composites discussed in Fig. 6. Phases 1, 2, 3 and 8 are associated with westerly wind anomalies dominating the tropics east of the date line including tropical South America and equatorial Atlantic, which explains the increase in the frequency of weak $ITCZ_{10-70}$ events relative to intense events in these phases. Interestingly, the relatively high frequency of intense $ITCZ_{10-70}$ events compared to weak events in phases 7 and 8 during the winter (Fig. 14d) cannot be explained by the MJO induced U850 wind anomalies over the equatorial Atlantic. However, the MJO circulation patterns in these phases indicate upper level divergence over the equatorial Atlantic off the coast of South America and convective anomalies over northern South America that could be somewhat linked to intensified convection in the ITCZ during the winter. We recall that circulation changes from winter to summer and the patterns of circulation shown in Jones (2009) and Jones and Carvalho (2011, 2012, 2014) are typical of the austral summer. In addition, the extratropical forcing associated with the coupled Kelvin–Rossby wave is not properly represented in composites averaged

around the equator as the ones shown in Jones (2009). This present study demonstrates that the extratropical forcing is essential for the enhancement (weakening) of convection in the $ITCZ_{10-70}$.

6 Summary and conclusions

This study examines mechanisms associated with the intraseasonal variability of the A-ITCZ during the austral summer (November–March) and winter (May–September) and investigates relationships with the MJO using CFS reanalysis and OLR. To objectively identify the A-ITCZ we propose a new index based on combined EOF analysis performed with anomalies (annual cycle and long-term trend removed) of atmospheric variables that are commonly used to identify the ITCZ in weather maps (i.e., precipitation, and zonal and meridional winds at 850 hPa). The first CEOF mode characterizes the dominant pattern of variability of the A-ITCZ around 5°N, and associates intensification in precipitation with enhanced convergence of the trade winds. The time-coefficient of the first CEOF was used as the A-ITCZ index. The advantage of this approach is that the index is temporally continuous and is not based on a single variable such as precipitation or circulation, but on the covariability of both. With this methodology we show that the A-ITCZ exhibits variations on a broad range of scales. On intraseasonal time-scales, the focus of this study, we observe that weak and intense $ITCZ_{10-70}$ events (defined when the index is below its 25th percentile and above its 75th percentile, respectively) occur approximately with the same probability in the winter and summer (on average, 5 events per season). The frequency of these events exhibits non-systematic relationship with ENSO and no trends in nearly 3 decades of analysis (1979–2010).

Variations in the ITCZ are essentially driven by the trade winds. The North and South Atlantic anticyclones play a major role in this process. We show that midlatitude wave trains modulate the characteristics of the anticyclones and, consequently, the intensity of the trade winds and strength of the convergence zone. This dynamical forcing is characterized by a midlatitude Rossby wave with equivalent barotropic structure. The winter hemisphere, where the subtropical jet is generally stronger, influences the Rossby wave that propagates equatorward following wave guides that depend on the jet (Hoskins and Ambrizzi 1993). The intensification of the convergence of the trade winds and enhancement of convection near the equator depend on the phase of the wave train as it propagates equatorward. The maximum convection in the $ITCZ_{10-70}$ occurs when the easterlies at 850 hPa dominate the tropics, independently on the season. More importantly, the mechanisms driving variations in the A-ITCZ also modulate convective

activity in large areas over Africa and South America and are linked to active and break phases of the monsoons in both continents.

Enhanced $ITCZ_{10-70}$ convection is associated with increased divergence in upper levels and atmospheric baroclinic structure near the equator. During austral summer, inter-hemispheric teleconnections are observed associated with barotropic-to-baroclinic transition of the wave train when convection peaks near the equator. There is indication that the main mechanism behind the inter-hemispheric teleconnection is the vertical shear over tropical South America and western South Atlantic characterized by easterly winds in low levels and westerly winds in upper levels. This mechanism has been examined with idealized experiments in Ji et al. (2014). Inter-hemispheric teleconnections are not evident in the austral winter, which is consistent with the weak vertical shear in the tropical NH shown in the composites of circulation in 850 and 200 hPa (Figs. 11, 13).

The MJO is a well-known mode of intraseasonal variability that modulates convection and circulation in the tropics and extratropics on intraseasonal time-scales (e.g., Zhang 2005). These teleconnection mechanisms are mainly explained by the MJO forced coupled Kelvin–Rossby wave response. We investigate the relationships between phases of the MJO and $ITCZ_{10-70}$ weak and intense events using the MJO index developed in Jones (2009). About 60 % of the $ITCZ_{10-70}$ weak and intense events investigated with our methodology occurred when the MJO was active during the austral summer compared with periods when the oscillation was inactive. During the austral winter the frequency of events during active MJO reduces to about 50 %, suggesting that other forcing mechanisms modulating the atmosphere on intraseasonal time-scales are as relevant as the MJO during this season. The phases of the MJO with strongest teleconnections with the $ITCZ_{10-70}$ intense events are the ones associated with the strengthening of the trade winds in the equatorial Atlantic. The MJO convective activity during intense events locates over western Pacific whereas suppression is observed over South America and Africa, consistent with the Rossby wave response shown in this study. Conversely, the phases of the MJO with teleconnection patterns that enhance the westerly winds in the equatorial Atlantic are related to $ITCZ_{10-70}$ weak events. These phases are associated with enhanced convection over Africa and South America. A direct association between the MJO Kelvin wave response and $ITCZ_{10-70}$ events is not examined here.

The variability of the A-ITCZ is notoriously complex and depends on the interaction among phenomena on a broad range of spatiotemporal scales. Fluctuations in convection on intraseasonal time-scales have large impact on population living in the Caribbean and coastal areas of South America that are directly affected by precipitation

regimes associated with the A-ITCZ. Additionally, mechanisms affecting the A-ITCZ also play significant role in modulating circulation and rainfall in large areas over tropical Africa and South America. This study provides a new framework to investigate the A-ITCZ on several time-scales, widens our understanding about mechanisms affecting the convergence zone and potentially contributes to advance weather and climate forecasts in low latitudes.

References

Asnani GC (1993) Tropical meteorology. Prof. CG Asnani, Pune

Becker EJ, Berbery EH, Higgins RW (2011) Modulation of cold-season U.S. daily precipitation by the Madden–Julian oscillation. J Clim 24:5157–5166. doi:10.1175/2011JCLI4018.1

Burpee RW (1972) The origin and structure of easterly waves in the lower troposphere of North Africa. J Atmos Sci 29:77–90

Burpee RW (1974) Characteristics of North African easterly waves during the summers of 1968 and 1969. J Atmos Sci 31:1556–1570

Carlson TN (1969) Some remarks on African disturbances and their progress over the Tropical Atlantic. Mon Weather Rev 97(10):716–726

Carvalho MAV, Oyama MD (2013) Variabilidade da largura e intensidade da Zona de Convergência Intertropical Atlântica: aspectos observacionais. Rev Bras Meteorol 28(3):305–316

Carvalho LMV, Jones C, Liebmann B (2002) Extreme precipitation events in southeastern South America and large-scale convective patterns in the South Atlantic convergence zone. J Clim 15:2377–2394

Carvalho LMV, Jones C, Liebmann B (2004) The South Atlantic convergence zone: intensity, form, persistence, and relationships with intraseasonal to interannual activity and extreme rainfall. J Clim 17:88–108

Carvalho LMV, Silva AE, Jones C, Liebmann B, Silva Dias PL, Rocha HR (2011) Moisture transport and intraseasonal variability in the South America monsoon system. Clim Dyn 36:1865–1880

Chatfield C (1996) The analysis of time series: an introduction. Chapman & Hall/CRC, New York

Chiang JCH, Kushnir Y, Giannini A (2002) Deconstructing Atlantic Intertropical Convergence Zone variability: influence of the local cross-equatorial sea surface temperature gradient and remote forcing from the eastern equatorial Pacific. J Geophys Res. doi:10.1029/2000JD000307

Citeau J, Finaud L, Cammas JP, Demarcq H (1989) Questions relative to ITCZ migrations over the tropical Atlantic Ocean, sea surface temperature and Senegal River runoff. Meteorol Atmos Phys 41:181–190

Cunningham CAC, Cavalcanti IFA (2006) Intraseasonal modes of variability affecting the South Atlantic convergence zone. Int J Climatol 26:1165–1180

De Souza EB, Ambrizzi T (2006) Modulation of the intraseasonal rainfall over tropical Brazil by the Madden–Julian oscillation. Int J Climatol 26:1759–1776

De Souza EB, Kayano MT, Ambrizzi T (2005) Intraseasonal and submonthly variability over the Eastern Amazon and Northeast Brazil during the autumn rainy season. Theor Appl Climatol 81:177–191

Diedhiou A, Janicot S, Viltard A, De Felice P, Laurent H (1999) Easterly wave regimes and associated convection over West Africa and tropical Atlantic: results from the NCEP/NCAR and ECMWF reanalyses. Clim Dyn 15:795–822

Enfield DB (1996) Relationships of inter-American rainfall to tropical Atlantic and Pacific SST variability. Geophys Res Lett 23(23):3305–3308

Gill AE (1980) Some simple solution for heat-induced tropical circulation. Q J R Meteorol Soc 106:447–462

Grodsky SA, Carton JA (2001) Coupled land/atmosphere interactions in the West African Monsoon. Geophys Res Lett 28(8):1503–1506

Gu G, Adler RF (2009) Interannual variability of boreal summer rainfall in the equatorial Atlantic. Int J Climatol 29:175–184

Hastenrath S, Lamb P (1977) Some aspects of circulation and climate over the eastern equatorial Atlantic. Mon Weather Rev 105:1019–1023

Hendon HH, Salby ML (1994) The life cycle of the Madden–Julian oscillation. J Atmos Sci 51(15):2225–2237

Hoskins BJ, Ambrizzi T (1993) Rossby wave propagation on a realistic longitudinally varying flow. J Atmos Sci 50(12):1661–1671

Hoskins BJ, Karoly DJ (1981) The steady linear response of a spherical atmosphere to thermal and orographic forcing. J Atmos Sci 38:1179–1196

Hsu H-H, Lin S-H (1992) Global teleconnections in the 250-mb streamfunction field during the Northern Hemisphere winter. Mon Weather Rev 120:1169–1190

Janicot S, Sultan B (2001) Intra-seasonal modulation of convection in the West African monsoon. Geophys Res Lett 28(3):523–526

Janowiak JE, Arkin PA, Morrisey M (1994) An examination of the diurnal cycle in oceanic tropical rainfall using satellite and in situ data. Mon Weather Rev 122:2296–2311

Ji X, Neelin JD, Lee S-K, Mechoso CR (2014) Interhemispheric teleconnections from tropical heat sources in intermediate and simple models. J Clim 27:684–697

Jones C (2009) A homogeneous stochastic model of the Madden–Julian oscillation. J Clim 22:3270–3288

Jones C, Carvalho LMV (2002) Active and break phases in the South American monsoon system. J Clim 15:905–914

Jones C, Carvalho LMV (2011) Stochastic simulations of the Madden–Julian oscillation activity. Clim Dyn 36:229–246

Jones C, Carvalho LMV (2012) Spatial-intensity variations in extreme precipitation in the contiguous United States and the Madden–Julian oscillation. J Clim 25:4898–4913

Jones C, Carvalho LMV (2014) Sensitivity to Madden–Julian oscillation variations on heavy precipitation over the contiguous United States. Atmos Res 147–148:10–26

Jones C, Schemm J-KE (2000) The influence of intraseasonal variations on medium-to extended-range weather forecasts over South America. Mon Weather Rev 128:486–494

Kiladis GN, Weickmann KM (1992) Extratropical forcing of tropical Pacific convection during northern winter. Mon Weather Rev 120:1924–1938

Knutson TR, Weickmann KM (1987) 30–60 Day atmospheric oscillations: composite life cycles of convection and circulation anomalies. Mon Weather Rev 115:1407–1436

Lau WK-M, Waliser DE (2012) Intraseasonal variability in the atmosphere–ocean climate system. Springer, New York

Liebmann B, Smith CA (1996) Description of a complete (interpolated) outgoing longwave radiation dataset. Bull Am Meteorol Soc 77(6):1275–1277

Liebmann B, Kiladis GN, Marengo JA, Ambrizzi T, Glick JD (1999) Submonthly convective variability over South America and the South Atlantic convergence zone. J Clim 12:1877–1891

Madden RA, Julian PR (1971) Detection of a 40–50 day oscillation in the zonal wind in the tropical Pacific. J Atmos Sci 28:702–708

Madden RA, Julian PR (1994) Observation of the 40–50 day tropical oscillation—a review. Mon Weather Rev 122:814–837

Maloney ED, Hartmann DL (1998) Frictional moisture convergence in a composite life cycle of the Madden–Julian oscillation. J Clim 11:2387–2403

Maloney ED, Shaman J (2008) Intraseasonal variability of the West African monsoon and Atlantic ITCZ. J Clim 21:2898–2918

Mathon V, Diedhiou A, Laurent H (2002) Relationship between easterly waves and mesoscale convective systems over the Sahel. Geophys Res Lett. doi:10.1029/2001GL014371

Matthews AJ (2000) Propagation mechanisms for the Madden–Julian oscillation. Q J R Meteorol Soc 126(569):2637–2651

Melo ABC, Cavalcanti IFA, Souza PP (2009) Zona de Convergência Intertropical do Atlântico. In: Cavalcanti IFA, Ferreira NJ, Justi da Silva MGA, Silva Dias MAF (eds) Tempo e Clima no Brasil. Oficina de Textos, São Paulo, pp 25–41

Mo KC, Ghil M (1987) Statistics and dynamics of persistent anomalies. J Atmos Sci 44:877–901

Mo KC, Higgins RW (1998) The Pacific-South American modes and tropical convection during the Southern Hemisphere winter. Mon Weather Rev 126:1581–1596

Mounier F, Janicot S, Kiladis GN (2008) The West African monsoon dynamics. Part III: the quasi-biweekly zonal dipole. J Clim 21:1911–1928

Moura AD, Shukla J (1981) On the dynamics of droughts in Northeast Brazil: observation, theory, and numerical experiments with a general circulation model. J Atmos Sci 38:2653–2675

Ninomiya K (2007) Similarity and difference between the South Atlantic convergence zone and the Baiu frontal zone simulated by an AGCM. J Meteorol Soc Jpn 85(3):277–299

Nobre P, Shukla J (1996) Variations of sea surface temperature, wind stress, and rainfall over the tropical Atlantic and South America. J Clim 9:2464–2479

Nogués-Paegle J, Byerle LK, Mo KC (2000) Intraseasonal modulation of South American summer precipitation. Mon Weather Rev 128:837–850

North GR, Bell TL, Cahalan RF, Moeng FJ (1982) Sampling errors in the estimation of empirical orthogonal functions. Mon Weather Rev 110:699–706

Quadro MFL, Silva Dias MAF, Herdies DL, De Gonçalves LGG (2012) Análise Climatológica da Precipitação e do Transporte de Umidade na Região da ZCAS através da Nova Geração de Reanálises. Rev Bras Meteorol 27(2):152–162

Reed RJ, Norquist DC, Recker EE (1977) The structure and properties of African wave disturbances as observed during Phase III of GATE. Mon Weather Rev 105:317–333

Rodrigues RR, Haarsma RJ, Campos EJD, Ambrizzi T (2011) The impacts of inter-El Niño variability on the Tropical Atlantic and Northeast Brazil climate. J Clim 24:3402–3422

Saha S et al (2010) The NCEP climate forecast system reanalysis. Bull Am Meteorol Soc 91(8):1015–1057

Silva VBS, Kousky V, Higgins W (2011) Daily precipitation statistics for South America: an intercomparison between NCEP reanalyses and observations. J Hydrometeorol 12:101–117

Souza P, Cavalcanti IFA (2009) Atmospheric centres of action associated with the Atlantic ITCZ position. Int J Climatol 29:2091–2195

Spiegel MR (1972) Schaum's outline of theory and problems of statistics. McGraw-Hill, São Paulo

Sultan B, Janicot S (2000) Abrupt shift of the ITCZ over West Africa and intra-seasonal variability. Geophys Res Lett 27(20):3353–3356

Sultan B, Janicot S (2003) The West African monsoon dynamics. Part II: the "Preonset" and "Onset" of the summer monsoon. J Clim 16:3407–3427

Sultan B, Janicot S, Diedhiou A (2003) The West African monsoon dynamics. Part I: documentation of intraseasonal variability. J Clim 16(21):3389–3406

Thompson RM Jr, Payne SW, Recker EE, Reed RJ (1979) Structure and properties of synoptic-scale wave disturbances in the tropical convergence zone of the Eastern Atlantic. J Atmos Sci 36:53–72

Tomas RA, Webster PJ (1994) Horizontal and vertical structure of cross-equatorial wave propagation. J Atmos Sci 51(11):1417–1430

Uvo CB, Nobre CA (1989) A Zona de Convergência Intertropical (ZCIT) e a precipitação no norte do Nordeste do Brasil. Parte I: a posição da ZCIT no Atlântico equatorial. Climanálise 4(7):34–40

Viltard A, De Felice P (1979) Statistic analysis of wind velocity in an easterly wave over West Africa. Mon Weather Rev 107:1320–1327

Viltard A, De Felice P, Oubuih J (1997) Comparison of the African and the 6–9 day wave-like disturbance patterns over West-Africa and the tropical Atlantic during summer 1985. Meteorol Atmos Phys 62:91–99

Wagner RG (1996) Decadal-scale trends in mechanisms controlling meridional sea surface temperature gradients in the tropical Atlantic. J Geophys Res 16:683–694

Waliser DE, Gautier C (1993) A satellite-derived climatology of the ITCZ. J Clim 6:2162–2174

Waliser DE, Somerville RCJ (1994) Preferred latitudes of the intertropical convergence zone. J Atmos Sci 51(12):1619–1639

Wallace JM, Gutzler TS (1981) Teleconnections in the geopotential height field during the Northern Hemisphere winter. Mon Weather Rev 109:784–812

Wang H, Fu R (2007) The influence of Amazon rainfall on the Atlantic ITCZ through convectively coupled Kelvin waves. J Clim 20:1188–1201

Webster PJ, Holton JR (1982) Cross-equatorial response to middle-latitude forcing in a zonally varying basic state. J Atmos Sci 39:722–733

Wheeler MC, Hendon HH (2004) An all-season real-time multivariate MJO index: development of an index for monitoring and prediction. Mon Weather Rev 132:1917–1932

Wilks DS (2006) Statistical methods in the atmospheric sciences. Academic Press, Burlington

Xie S-P, Philander GR (1994) A coupled ocean–atmosphere model of relevance to the ITCZ in the eastern Pacific. Tellus A 46(4):340–350

Yang G-Y, Slingo J (2001) The diurnal cycle in the tropics. Mon Weather Rev 129:784–801

Zhang C (2005) Madden–Julian oscillation. Rev Geophys 43:RG2003. doi:10.1029/2004RG000158

Zhou J, Lau K-M (2001) Principal modes of interannual and decadal variability of summer rainfall over South America. Int J Climatol 21:1623–1644